THE JOURNAL OF PHYSICAL CHEMISTRY A

Article

pubs.acs.org/JPCA

Determination of Absolute Configuration in Chiral Solvents with Nuclear Magnetic Resonance. A Combined Molecular Dynamics/Quantum Chemical Study

Jiří Kessler,[†,‡] Martin Dračínský,[†] and Petr Bouř*[,†]

[†]Institute of Organic Chemistry and Biochemistry, Academy of Sciences, Flemingovo náměstí 2, 166 10 Prague, Czech Republic

[‡]Department of Physical and Macromolecular Chemistry, Faculty of Science, Charles University, Hlavova 8, 128 40 Prague, Czech Republic

Supporting Information

ABSTRACT: Nuclear magnetic resonance (NMR) spectroscopy is omnipresent in chemical analysis. However, chirality of a molecule can only be detected indirectly by NMR, e.g., by monitoring its interaction with another chiral object. In the present study, we investigate the spectroscopic behavior of chiral molecules placed into a chiral solvent. In this case, the solvent−solute interaction is much weaker, but the application range of such NMR analysis is wider than for a specific chemical shift agent. Two alcohols and an amine were used as model systems, and differences in NMR chemical shifts dependent on the solute−solvent chirality combination were experimentally detected. Combined quantum mechanic/molecular mechanic (QM/MM) computations were applied to reveal the underlying solute−solvent interactions. NMR shielding was calculated using the density functional theory (DFT). While the experimental observations could not be reproduced quantitatively, the modeling provided a qualitative agreement and detailed insight into the essence of solvent−solute chiral interactions. The potentials of mean force (PMF) obtained using molecular dynamics (MD) and the weighted histogram analysis method (WHAM) indicate that the chiral interaction brings about differences in conformer ratios, which are to a large extent responsible for the NMR shifts. The MD results also predicted slight changes in the solvent structure, including the radial distribution function (RDF), to depend on the solvent/solute chirality combination. Apart from the conformer distribution, an effective average solvent electrostatic field was tested as another major factor contributing to the chiral NMR effect. The possibility to simulate spectral effects of chiral solvents from the first-principles opens up the way to NMR spectroscopic determination of the absolute configuration for a larger scale of compounds, including those not forming specific complexes.

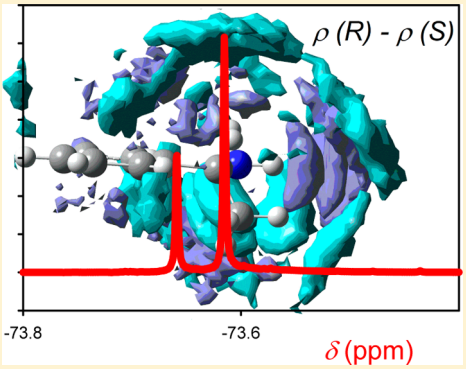

INTRODUCTION

Life on Earth depends on a mutual recognition and interaction of a vast number of molecules that exhibit the left- and right-hand "chiral" or "helical" symmetry. Directly, molecular chirality, i.e., the absolute configuration (AC), can be determined by X-ray crystallography,[1] or by spectroscopic methods taking advantage of the differences in scattering or absorption of left- or right- circularly polarized light.[2] In particular, the latest developments in the field of vibrational optical activity[3] (VOA) made this process fairly easy for small molecules in solutions: the compounds do not have to be crystallized, and first-principles computations became accurate enough to enable a reliable interpretation of the spectra.[4,5]

Nuclear magnetic resonance (NMR) based on interaction of nuclei with an electronic cloud and an external magnetic field often provides higher resolution, higher sensitivity, and a broader application potential than the optical spectroscopic methods. Unfortunately, conventional NMR experiment is insensitive to chirality.[6] A perturbation of the axially symmetric magnetic field by additional electromagnetic components was suggested to rectify it, but it is not widely used.[6−8] Instead, covalent derivatization with an auxiliar chiral reagent or complexation of the studied compounds with suitable chiral solvents or chiral shift reagents is more common, as an economic and easy way to treat the chirality problem in NMR.[9−12]

Chiral solvating agents (CSA) associate with the substrate through noncovalent interactions, but generally undergo fast exchange with individual substrate molecules.[13] The most important factor determining the induced shifts is the strength of the mutual interaction.[14] Many different molecules have been used as CSA including acids, amines, alcohols, sulfoxides, and cyclic compounds. Chiral solvents often induce chemical shift changes in solutes as a result of strong polar interaction as well. Optical purity ("enantiomeric excess") in enantiomeric

Special Issue: Jacopo Tomasi Festschrift

Received: October 2, 2014
Revised: November 14, 2014
Published: November 20, 2014

   dx.doi.org/10.1021/jp509988e | J. Phys. Chem. A 2015, 119, 5260−5268

mixtures can be conveniently obtained by a simple integration of NMR peaks corresponding to the two components. However, there is no direct way to determine AC by these techniques without an additional calibration.

Another standard approach to fully determine AC by NMR involves derivatization of the substrate (i.e., a pure enantiomer) with two enantiomers of a chiral derivatizing agent (CDA), producing two diastereomeric derivatives.[15,16] The chiral environment is thus provided by the auxiliary reagent. Many CDAs useful in assigning the AC of different substrates have been developed.[9] As an example, we should mention at least the most successful Mosher's method, which uses the α-methoxy-α-trifluoromethylphenylacetic acid as CDA.[17] A severe disadvantage of the CDA approaches lies in the fact that the substrate must be modified by covalent binding, which is not always possible or desirable.

In the present study, we explore NMR chemical shift differences caused in enantiomeric compounds by a chiral solvent. Although such chiral mixtures can be readily resolved in theory, the resultant chemical shift changes are small in the absence of a strong solvent−solute interaction, and to the best of our knowledge, they were not used for AC determination so far.

For our model compounds, simple chiral alcohols and an amine, we did observe splitting of NMR lines. Solutes of the R and S configuration dissolved in a chiral solvent (say of the R configuration) provided different NMR chemical shifts. To understand the splitting, we performed molecular dynamics (MD) simulations that indicated the underlying structural differences due to the weak chiral interactions, consisting of perturbed conformer equilibria and the structure of the first solvation shell.

It turned out that rather long simulation times were needed to capture the weak interactions by MD, and direct averaging of the clusters (snapshots) was not possible. However, MD simulations revealed fine differences in the solute and solvent structure. We therefore separately estimated chiral splitting of the chemical shift as caused by perturbed conformer equilibria, and by an effective electrostatic solvent potential. The density functional theory (DFT) computations then provided chemical shift differences, comparable in magnitude with the experiment. MD simulations also indicated a possible mechanism of the chirality recognition. We thus consider the findings important for further development of chiral NMR spectroscopy, as they provide both insight and a quantitative description of the weak chiral intermolecular interactions.

METHODS

Experimental Details. Both enantiomers of the three model compounds, 2,2,2-trifluoro-1-phenylethanol (**1**), 1-phenylethanol (**2**), and 1-phenylethanamine (**3**) (Figure 1) were purchased from Sigma-Aldrich. NMR spectra were measured on a Bruker Avance II 500 spectrometer (499.8 MHz for ^{1}H, 125.7 MHz for ^{13}C and 470.3 MHz for ^{19}F). A mixture of 50 μL of one enantiomer and 25 μL of the other enantiomer was dissolved in 500 μL of a pure enantiomer of the solvent, so that the signals could be easily identified from the relative NMR peak areas. For the ^{13}C spectra, the attached proton test (APT) sequence was applied for an easier carbon assignment. No deuterated solvents were used and the magnetic field homogenity was shimmed manually.

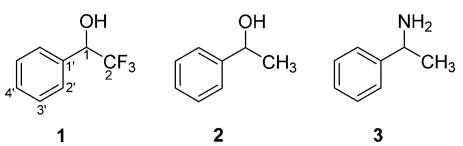

Figure 1. Studied compounds: 2,2,2-trifluoro-1-phenylethanol (**1**, with atom numbering), 1-phenylethanol (**2**), and 1-phenylethanamine (**3**).

Molecular Dynamics. Because of the relatively low concentration of the solute in the experiment, we neglected interactions between solute molecules in the modeling. One solute and 49 solvent molecules were placed in a cubic box. The box was 22.06 Å, 22.43 Å, 22.06 Å, and 22.43 Å long for the **1@3**, **3@1**, **2@3**, and **2@1** systems, respectively. **1@3** denotes solute **1** dissolved in solvent **3**, etc. For each system, all four R@R, R@S, S@S, and S@R chirality combinations were investigated under the same conditions, which provided an additional check of computational accuracy: energies of the R@R system should be the same as those of S@S, the R@S is energetically equivalent to S@R.

Free MD simulations were performed using the General Amber force field (GAFF)[18] and the Amber simulation package.[19] Some test computations were also performed with the Gromacs program[20] and the same force field; they provided similar results as Amber (data not shown). Each production computation 400 ns long was preceded by a minimization and 10 ns equilibration run, using the *NVT* ensemble, temperature 300 K, and time integration step 1 fs. The geometry snapshots saved in regular 1 ps intervals were analyzed by Amber's and our own program's scripts.

The potential of mean force (PMF, i.e., the free energy F for the *NVT* ensemble) as a function of the $C_{1'}-C_1-O-H$ (for **1** and **2**) or $C_{1'}-C_1-N-H$ (for **3**) torsion angles (Figure 1) was determined using the weighted histogram analysis method (WHAM).[21] Eleven histograms within the $-180°\cdots180°$ interval were constructed, each of them based on 400 ns runs, while applying harmonic potential restraints with a force constant of 0.0018 kcal·mol^{-1} deg^{-2}. The Wham program (http://membrane.urmc.rochester.edu/content/wham) was employed to process the Amber output. To avoid an occasional umbrella-like flipping of the C_1-NH_2 group in **3** during the dynamics, two harmonic potential restraints, each with a force constant of 0.0018 kcal·mol^{-1} deg^{-2}, were applied to restrict the two $C_1-H-N-H$ torsion angles (i.e., with a virtual C_1-H bond).

We were also interested in the effective electrostatic field sensed by the solute and chiral solvent, and its consequences for NMR shielding. Control computations indicated a reasonable correlation between isotropic shielding and solvent electrostatic potential (Figure S1). Also previous works document the importance of the electrostatic potential for spectral properties.[22,23] Therefore, in the last set of MD simulations, average solvent electrostatic potentials measured at solute's atoms were calculated for frozen solute conformers of the B3LYP/6-311++G**/PCM optimized geometry. The atoms were fixed in space via a harmonic potential (force constant 1000 kcal·mol^{-1} Å^{-2}). For each conformer, the potential was calculated from 400 ns MD trajectory. The conformer was then placed in a cavity created by the Gaussian program[24] and the polarizable continuum solvent model[25] (PCM). Using our own programs, a charge was put on each tessera of the cavity surface to reproduce the calculated MD potentials. Least-square fitting procedure was used for the charge estimation, and the sum of the charges was set to zero.

dx.doi.org/10.1021/jp509988e | J. Phys. Chem. A 2015, 119, 5260−5268

Table 1. Calculated Relative Energies (kcal/mol) and Characteristic Torsional Angles[a] (deg.) of the Lowest Energy Conformers

	B3LYP-D 6-311++G** CPCM		*E*									PMF[b]	B3LYP-D 6-311++G** CPCM		
conformer	φ_{OH}	φ_{Phe}	HF 6-31G	HF 6-31G**	MP2 6-31G**	B3LYP 6-31G**	B3LYP 6-311++G**	B3LYP 6-311++G** CPCM	B3LYP-D 6−311++G** CPCM	MP2 6-311++G** CPCM	B3LYP-D aug-cc-pVTZ CPCM	GAFF	*F*	ZPE	*H*	*G*
Compound R-**1**																
I	−173	−38	0.00	0.00	0.00	0.00	0.00	0.00	0.00	0.00	0.00	0.43	1.04	0.00	0.00	0.00
II	48	−56	1.56	1.63	1.34	1.13	1.02	0.67	0.35	0.77	0.39	1.15	1.60	0.43	0.42	0.81
III	−55	−42	0.70	0.58	0.99	1.00	0.96	0.35	0.47	0.34	0.48	0.00	0.00	0.25	0.36	0.28

	B3LYP-D 6-311++G** CPCM		*E*			PMF[b]	B3LYP-D 6-311++G** CPCM		
conformer	$\varphi_{OH}/\varphi_{\langle NH\rangle}$	φ_{Phe}	B3LYP-D 6-311++G** CPCM	MP2 6-311++G** CPCM	B3LYP-D aug-cc-pVTZ CPCM	*F*	ZPE	*H*	*G*
Compound R-**2**									
I	55	46	0.00	0.00	0.00	0.00	0.00	0.00	0.00
II	−174	43	0.91	1.07	0.82	0.81	0.81	0.84	0.73
III	−72	22	1.00	1.30	0.88	0.83	1.18	1.08	1.41
Compound R-**3**									
I	−13	56	0.00	0.33	0.00	0.00	0.00	0.00	0.00
II	121	47	0.09	0.00	0.09	0.11	0.06	0.02	0.27
III	−119	−65	0.97	1.34	0.91	0.36	0.93	0.93	1.08

[a]B3LYP-D/6-311++G**/CPCM, $\varphi_{OH} = \angle C_{1'}C_1OH$, $\varphi_{Phe} = \angle C_{2'}C_{1'}C_1O$, and average $\varphi_{\langle NH\rangle} = \angle C_{1'}C_1NH$ angle, cf. Figure 1. *E*, *F*, ZPE, *H*, and ΔG are the electronic, free, and zero-point energy, enthalpy and Gibbs' energy, respectively. [b]From MD for the **1@3**, **3@1**, and **2@1** systems.

dx.doi.org/10.1021/jp509988e | J. Phys. Chem. A 2015, 119, 5260−5268

Table 2. Selected Isotropic Shielding (ppm) Calculated for Individual Conformers[a]

	Compound 1								
basis, number of basis functions	6-31G 122	6-31G** 215	IGLOII 318	6-311++G** 325	IGLOIII 514	$IGLOIII_{HF}$ 514	$IGLOIII_{MP2}$ 514	6-311++G (2df,2pd) 580	aug-cc-pVTZ 835
Conformer I									
H_1 (α)	−27.96	−26.83	−27.01	−26.80	−26.44	−27.02	−24.90	−26.34	−26.30
F	−266.27	−276.76	−256.72	−252.51	−251.65	−299.30	−286.03	−255.94	−256.72
C_1 (α)	−118.49	−115.27	−101.62	−103.05	−97.10	−120.70	−115.31	−99.52	−100.52
$C_{1'}$	−64.45	−60.20	−38.78	−40.00	−32.06	−47.33	−53.36	−36.19	−35.53
Conformer II − Conformer I									
H_1 (α)	−0.24	−0.38	−0.36	−0.38	−0.43	−0.23	−0.77	−0.41	−0.42
F	−1.21	−0.98	−0.15	0.21	0.11	0.33	0.64	0.11	0.14
C_1 (α)	−1.02	−0.60	−0.41	−0.26	−0.26	−0.09	−1.44	−0.24	0.16
$C_{1'}$	−0.13	−0.21	−0.06	−0.21	−0.19	0.37	−0.87	−0.25	−1.46
Conformer III − Conformer I									
H_1 (α)	−0.04	−0.07	−0.06	−0.10	−0.05	0.20	0.01	−0.06	−0.04
F	−3.44	−3.07	−2.94	−2.07	−2.15	−1.90	−2.27	−1.98	−1.87
C_1 (α)	−1.20	−0.99	−0.80	−0.76	−0.65	−0.39	−0.16	−0.66	−0.37
$C_{1'}$	−1.72	−2.15	−2.73	−2.53	−2.88	−2.41	−4.33	−2.54	−3.24

	Compound 2			Compound 3		
Conformer:	I	"II − I"	"III − I"	I	"II − I"	"III − I"
H_1 (α)	−26.87	0.14	0.09	−28.01	0.66	0.06
H_2 (Me)	−30.42	0.03	0.07	−30.49	0.10	0.10
C_1 (α)	−99.64	−0.04	−2.26	−119.78	−2.60	0.39
C_2 (Me)	−152.60	4.42	3.05	−152.39	0.08	4.32
$C_{1'}$	−20.27	−2.37	−0.43	−16.11	−7.34	−4.56
$C_{3'}$	−42.88	−0.31	−0.38	−42.73	−4.13	0.03

[a]For atoms relevant to the experiment, the B3LYP-D/IGLO III/CPCM method was used, unless indicated otherwise, for 6-311++G**/CPCM geometries.

The cavities contained a large number, about 1500 tesserae, and thus the charges could very faithfully reproduce the fine potential differences on solute atoms as caused by the differences in solvent chirality.

Density Functional Computations. DFT computations performed within the Gaussian program package were used to estimate relative conformer energies and isotropic NMR shielding. Systematic conformer searches with respect to the φ_{OH} = ∠$C_{1'}$−C_1−O−H and φ_{Phe} = ∠$C_{2'}$−$C_{1'}$−C_1−O angles were performed. For the amine (**3**), the $\varphi_{\langle NH\rangle}$ angle, analogous to φ_{OH}, was defined as an average of two $C_{1'}$−C_1−N−H angles. $\varphi_{\langle NH\rangle}$ is thus related to a line running in the middle of the two N−H bonds. Butylamine parameters were used for the solvent, as its size and the dielectric constant ε_r = 4.6178 are comparable to those of our model molecules. The UFF[26] atomic radii were used for the cavity construction. In some computations, the Grimme dispersion correction[27] was applied to the B3LYP[28] functional, which is denoted by the D letter as "B3LYP-D". The isotropic shielding was calculated at various approximation levels as specified below, using the gauge invariant atomic orbitals (GIAO)[29] and continuum-like solvent model (COSMO, its Gaussian version being referred to as CPCM).[30]

RESULTS AND DISCUSSION

Conformer Energies and NMR Shielding. Relative conformer energies calculated at different levels of approximation are summarized in Table 1. For **1**, a larger number of quantum-chemical methods is presented, to develop a feeling for the overall accuracy. They provide a relatively consistent ordering of the three lowest-energy conformers. In the lowest-energy conformer I, the OH group approximately points toward the CF_3 moiety, being partially stabilized by the OH···F intramolecular hydrogen bond. A fourth high-energy conformer not included in Table 1 was also found in low-level vacuum calculations; however, its relative energy was high, and it was not stable in the CPCM solvent environment. For conformers I−III, the solvent just appears to lower the energy differences between the conformers. The roles of the dispersion (cf. HF/6-31G** vs MP2/6-31G**) and vibrational corrections (*E* vs ZPE, *H*, Δ*G*) appear minor with respect to the conformer ordering. On the other hand, the empirical correction ("-D") changes the relative conformer ordering in case of the B3LYP/6-311++G**/CPCM method. PMF values obtained from MD provide unique ordering, preferring conformer III, unlike all the quantum-chemical approaches. This inconsistency can be most probably explained by inaccuracy of the GAFF force field. Especially the fluorine atoms may not be adequately described by GAFF. Indeed, already for a single molecule in vacuum (the "GAFF" column), the force field does not provide conformer ordering with the more accurate quantum-chemical method.

For the other compounds (**2** and **3**), three lowest-energy conformers were found as well. Similar performance of the computational methods was observed as for **1**; only some of them are thus listed in Table 1.

The lowest-energy conformer of **2** has a different orientation of the OH group than in compound **1**, because of the different

dx.doi.org/10.1021/jp509988e | J. Phys. Chem. A 2015, 119, 5260−5268

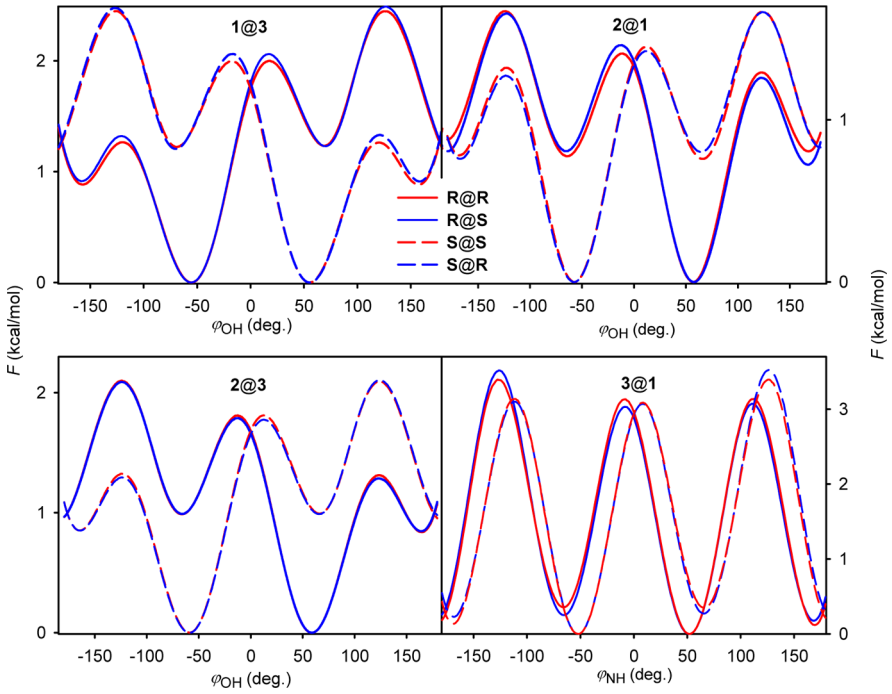

Figure 2. PMF profiles for the studied systems (obtained by WHAM, *NVT* dynamics, 11 histograms ×400 ns, and GAFF force field).

polarity of the CH_3 and CF_3 groups. Conformer I of **1** may be viewed as an analogue of II of **2**, etc. A more detailed inspection also reveals differences in the orientation of the phenyl group. For **3**, in the lowest energy conformer the free electron pair of nitrogen points approximately in the opposite direction as the phenyl group; however, the relative energy of the second conformer is quite close to that of the first one.

For selected atoms the calculated isotropic NMR shieldings, $\sigma = (\sigma_{xx} + \sigma_{yy} + \sigma_{zz})/3$, are summarized in Table 2. Many basis sets were used for compound **1**, to document a significant dependence of the shielding on the basis set used, and an often problematic convergence of the results. For example, the IGLOII and IGLOIII basis sets often recommended for NMR parameters[31] provide σ_F values of −256.72 and −251.65 ppm, respectively, at the B3LYP-D/CPCM level. The much larger and computationally more demanding aug-cc-pVTZ basis set provides a value of −256.72 ppm (same as the small IGLOII basis set result), etc. Even larger variance is caused by the change of the ab initio model: for σ_F and the IGLOIII basis set, values of −251.65, −299.30, and −286.03 ppm were obtained by the B3LYP, HF, and MP2 method, respectively. This is certainly not favorable for a reproduction of the small experimental chemical shift variations.

Fortunately, the relative isotropic shielding differences between individual conformers vary less than the absolute values. Even their signs are reproduced mostly consistently with various methods. The HF results (with the IGLOIII basis set) are very different from those obtained by B3LYP and MP2. The largest difference between the B3LYP and MP2 methods (−2.88 vs −4.33 ppm, IGLOIII basis set) is exhibited by the C_1 atom in conformer III. Within B3LYP, the signs of the differences appear stabilized for 6-311++G** and larger basis sets; the IGLOIII basis set was used for further chemical shift simulations.

Because the energy differences between the conformers are comparable to the Boltzmann factor ($kT \sim 0.6$ kcal/mol for 300 K) all three solute molecules exist in a conformer equilibrium in solution. The conformers exhibit distinct isotropic NMR shielding. Chemical shifts may thus depend on relative conformer ratios varying with the chirality of the environment. The energetics of the chiral solute-vs chiral-solvent interaction is explored in the next section by MD.

Potentials of Mean Force. Unlike the intrinsically achiral CPCM solvent model, MD simulation with explicit molecules is able to capture solvent chirality. This is documented in Figure 2 for all of the four investigated systems. The PMF profiles are plotted for all chirality combinations (R@R, R@S, S@S, and S@R), as dependent on the φ_{OH} angle (φ_{NH} for **3**; note that φ_{NH} for one hydrogen atom is not equal to the average $\varphi_{\langle NH\rangle}$ angle used for the conformer characterization). As expected, PMFs, and in particular the minima—the relative conformer energies—of the R@R system are the same as in S@S, and those of R@S and S@R are the same. The $\varphi_{OH}/\varphi_{NH}$ angles at PMFs minima (listed in Table 3) approximately correspond to the B3LYP-D/6-311++G**/CPCM values in Table 1. For example, for **1@3**, the −164°, 70°, and −52° values obtained by WHAM for the R-enantiomer correspond to the DFT values of −173°, 48°, and −55°, respectively, etc. The differences can be attributed to the lack of explicit solvent−solute interactions in PCM, and errors of the GAFF force field.

Because of the chiral interactions, the PMF profiles for the R@S and R@R systems are different, and the differences correspond to those found in the simulations of opposite chirality, i.e., S@R vs S@S. For example, in **1@3**, the relative energies of conformer I ($|\varphi_{OH}| = 164°$) are slightly higher for the S@R and R@S systems (blue curves) than for R@R and S@S (red), etc. All these free energy differences are summarized in Table 3; the largest one is 0.107 kcal/mol for conformer III of **2@1**. These differences in conformer energies lead to variations of conformer populations, as summarized in the last column of Table 3.

We note that relatively long WHAM simulations (4×10^8 steps) are needed to reproduce the small energy differences. Figure S2 documents the overall convergence of the relative

dx.doi.org/10.1021/jp509988e | J. Phys. Chem. A 2015, 119, 5260−5268

Table 3. Conformer φ_{OH} Values, Differences in Relative Energies (F, PMFs) and Population Differences η due to the Chirality

conformer	φ (deg)[a]	$F_{R@R\text{-}R@S}$ (kcal/mol)[b]	$\eta_{R@R\text{-}R@S}$ (%)[b]
1@3			
I	−164	−0.025	0.54
II	70	0.021	−0.21
III	−52	0.000	−0.33
2@1			
I	54	0.000	−1.37
II	−170	0.058	1.10
III	−72	0.107	0.27
2@3			
I	54	0.000	0.50
II	−170	0.052	−0.30
III	−72	−0.036	−0.20
3@1			
I	−16	0.000	0.31
II	110	0.079	−4.12
III	−93	−0.087	3.81

[a] φ_{OH} and $\varphi_{\langle NH\rangle}$, for R-enantiomers. [b] Averages from two complementary simulations, i.e., $F_{R@R\text{-}R@S} = (F_{R@R} - F_{R@S} + F_{S@S} - F_{S@R})/2$.

PMF conformer energy perturbations caused by the chirality; clearly, the differences smaller than about 0.01 kcal/mol are difficult to reproduce. In particular, for **1@3** and **2@3**, the PMF differences listed in Table 3 are comparable to the error of the method. On the other hand, compound **1** used as a solvent enables a clear discrimination between enantiomeric solute components, with the energy differences reaching up to ∼0.1 kcal/mol.

Differences in the Solvation Sphere Structure as Caused by Chirality. Similar to the perturbations of PMFs, solvents of opposite chirality differ in the structure of the solvation sphere. An example of the radial distribution function and the influence of the chiral environment is given in Figure 3,

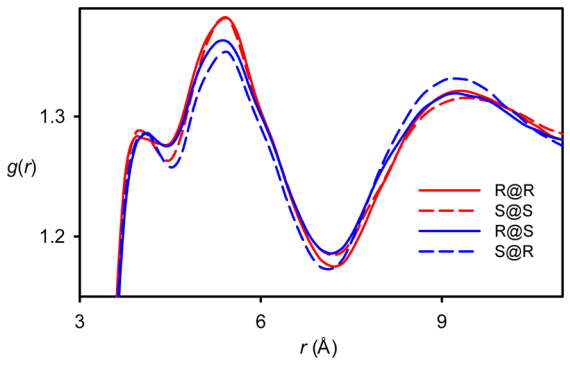

Figure 3. Radial distribution function in four **2@1** systems, as measured from the C_2 atom, and obtained from 200 ns MD runs.

for the **2@1** simulation. The "isochiral" R@R and S@S solute−solvent combinations provide distinct dependencies, namely, around the distance of $r \sim 6$ Å, which reflects the strongest solvent−solute interactions in the first hydration sphere. The convergence of integral chiral differences with respect to the number of the integration steps is documented in Figure S3. Similarly as for PMFs, a relatively long, at least 150 ns run is needed for a reliable estimation of the chiral environment's effects on the radial distribution function.

The differences in the radial distribution function do not correlate well with the observed NMR shift changes on individual atoms (Figure 4). One might expect that big

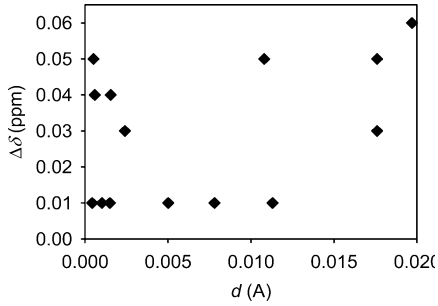

Figure 4. Experimental "R@S−R@S" chemical shift differences ($\Delta\delta$) vs differences in the radial distribution functions (d) of relevant atoms (absolute values, for all the **1@3**, **2@3**, and **2@1** and **3@1** systems, $d = 1/4\int_{d_1}^{d_2}[(g_{S@S} - g_{R@S})^2 + (g_{S@S} - g_{S@R})^2 + (g_{R@R} - g_{R@S})^2 + (g_{R@R} - g_{S@R})^2]dr$, $d_1 = 3$ Å, $d_2 = 11$ Å).

differences in NMR will in general correspond to big differences in the solvent structure around a particular atom, but Figure 4 suggests that the relationship is likely to be more complex than a direct proportionality.

An alternative insight into the mechanism of the chiral solvent−solute interactions is provided by the differences in solvent densities around a solute as plotted in Figure 5. For better accuracy, the difference density for the S solute enantiomer was inverted and averaged with that obtained for

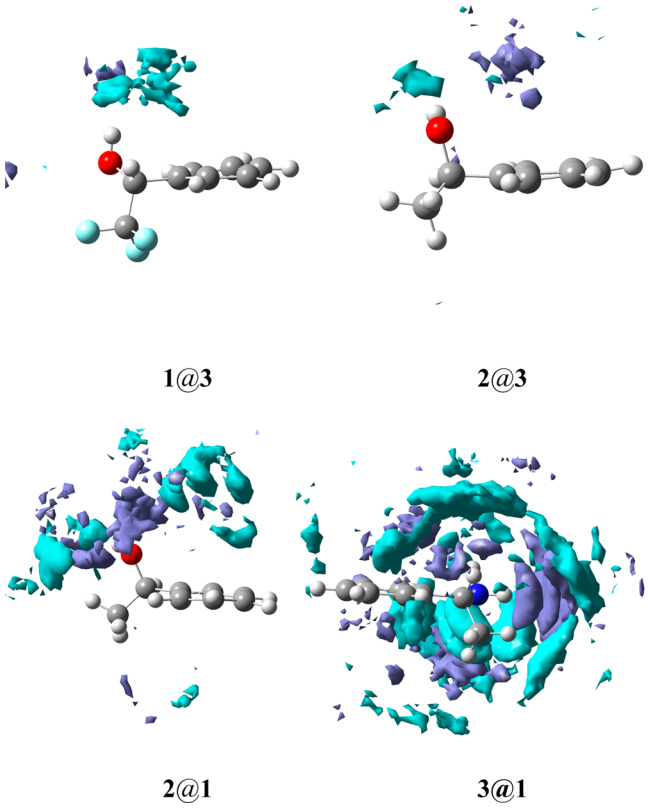

Figure 5. Calculated differences in solvent densities (isosurface at 0.01 g/mL), caused by the different chirality, averages from the "R@R−R@S" and "S@S−S@R" systems.

dx.doi.org/10.1021/jp509988e | J. Phys. Chem. A 2015, 119, 5260−5268

the R enantiomer. Individual difference densities exemplified in Supporting Information Figure S4 for the **1@3** system reveal a limited accuracy, but the "mirror image" density distribution is clearly apparent.

The density variations thus suggest, for example, that the alcohols **1** and **2** discriminate the chiral solvents mostly via an interaction with the OH and phenyl groups, as the density difference is located mostly around them. Both compounds interact strongly with the solvent, either via hydrogen bonds, or van der Waals forces. For the **2@1** system, an important participation of the methyl group is indicated by the density difference in its vicinity as well (Figure 5). For the amine in the **3@1** system, the difference density is more evenly spread around the solute, perhaps reflecting the less-directional polar interaction of the NH_2 group, compared to OH. On the other hand, for the fluorinated compound **1**, the density differences in the **1@3** system are most localized, which may be a consequence of its relatively large dipole moment, about twice as big as for the other two compounds.

By analysis of MD trajectories, we could also determine average solvent−solute contact times, i.e., times that a solvent molecule spends in the solute solvation sphere. These were for all systems nearly identical, close to 0.3 ps, albeit with large RMS deviations of 1.5−3.0 ps (Table S1). The dynamics thus does not indicate formation of stable solvent−solute complexes. This is consistent with the dispersed density patterns (Figure 5) and small chemical shift differences.

Solvent Electrostatic Potential and a Comparison to Experiment. So far, we explored how the chiral environment changes chemical shielding of the solute by affecting conformer populations. However, NMR properties of one particular conformer and its interaction with the solvent (not necessarily complex-like, cf. Table S1) can also reflect the environmental chirality. Currently we are not able to capture the solvent−solute interaction entirely, i.e., including possible charge-transfer, van der Waals interactions, etc. For example, a direct "brute force" averaging of MD clusters did not converge on a reasonable time scale. Therefore, we modeled the effect of the solvent via the averaged electrostatic potential. Obtaining reliable potential differences caused by chirality required a reasonably high number of MD steps, as documented in Figure S5 for conformer III of compound **1**, when compound **3** was used as a solvent. It is obvious that the main potential trends are apparent already at ∼50 ns of the MD run. Not surprisingly, the largest differences (∼0.5 V) are mostly associated with atoms close to the polar part of the molecule and its chiral center.

The approximation of the solvent effect by an electrostatic potential is justified by the domination of the electrostatic forces in the intermolecular interactions. Indeed, several previous studies indicate that the solvent electrostatic potential measured at the solute atomic nuclei well-reproduce the influence of polar solvents on solute spectroscopic properties.[23,32,33] The chemical shift correction obtained via the average solvent electrostatic potential and partial atomic charges was added to the calculated chemical shift differences. However, there is no apparent correlation between the differences in potentials and chemical shifts for the R@R and R@S systems (Figure S6), indicating that the electrostatic influence is not a dominating factor.

In Table 4, we compare the experimental differences with both the raw chemical shielding differences calculated from the different conformer distributions (3rd and fourth columns), and the sums containing the electrostatic correction (columns 5 and 6). Only experimental data in which the chiral splitting could be clearly identified in the NMR spectra are used, as shown, e.g., for the **1@S-3** system in Figure 6 containing parts of the all ^{1}H, ^{13}C, and ^{19}F spectra. The most illustrative splitting of −0.044 ppm belongs to ^{19}F (Figure 6c); the relative peak

Table 4. Calculated (B3LYP/IGLOIII/CPCM) and Experimental Chemical Shift Differences for Solutes of Mixed Chirality ($\Delta = \delta_S - \delta_R$ (ppm)) in Chiral Solvents[a]

system	atom	Δ_{MD}	Δ_{DFT}	$\Delta_{MD,\,Q}$	$\Delta_{DFT,\,Q}$	$\Delta_{Exp.}$
1@S-3	H_1 (α)	0.001	0.003	−0.013	0.012	−0.010
	F	0.007	0.011	0.054	−0.072	−0.044
	C_1 (α)	0.003	0.006	0.042	−0.032	−0.042
	$C_{1'}$	0.010	0.018	0.032	0.048	−0.028
2@R-1	H_1 (α)	0.001	0.002	0.004	0.006	−0.050
	H_2 (Me)	0.000	0.000	−0.002	−0.002	0.005
	C_1 (α)	0.024	0.011	0.011	−0.010	−0.048
	C_2 (Me)	0.027	0.051	0.051	0.070	0.06[b]
	$C_{1'}$	−0.028	−0.033	−0.061	−0.056	0.05[b]
2@S-3	H_1 (α)	−0.001	−0.002	0.005	0.008	−0.012
	H_2 (Me)	−0.000	−0.000	−0.001	−0.000	−0.002
	C_2 (Me)	−0.020	−0.074	−0.010	−0.063	−0.043
3@R-1	H_1 (α)	0.023	0.017	0.014	0.020	−0.037
	H_2 (Me)	0.000	0.002	0.017	0.011	0.008
	C_1 (α)	−0.123	−0.097	−0.043	−0.023	−0.017
	$C_{3'}$	−0.172	−0.143	−0.162	−0.255	−0.010

[a]The differences are calculated for MD (Δ_{MD}) and DFT (Δ_{DFT}, B3LYP/6-31++G**/CPCM free energies (ΔG)) Boltzmann populations perturbed by chiral environment, values including the electrostatic corrections are denoted by "Q". [b]Lower resolution due to signal overlap

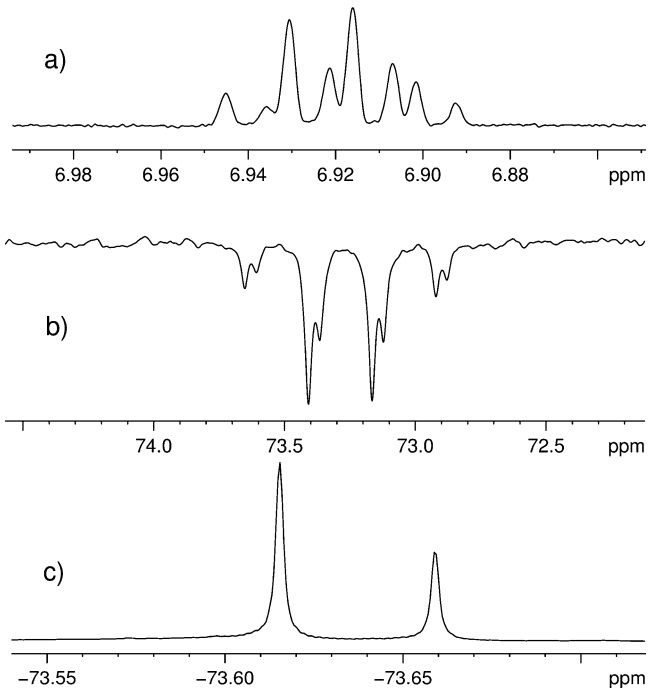

Figure 6. ^{1}H (a), ^{13}C (b), and ^{19}F (c) NMR spectra of a 2:1 mixture of R and S enantiomers of compound **1** dissolved in **3**. Only the aliphatic CH signals are shown in the hydrogen and carbon spectra; the attached proton test (APT) sequence was used for the ^{13}C experiment, providing the negative signal.

dx.doi.org/10.1021/jp509988e | J. Phys. Chem. A 2015, 119, 5260−5268

areas at −73.616 and −73.660 ppm (2:1) correspond to the S and R enantiomer of **1**.

Overall, in Table 4 we can see that the magnitudes of the computed shifts do agree with the observations; hence the differences in the conformer populations and effective solvent electrostatic field appear as the likely factors explaining the experimental data. On the other hand, the correlation between the calculated and experimental values is very weak. The differences between the computational results and the measured chemical shift differences are explicable by a combination of errors stemming from the quantum-mechanical model (functional, basis set), molecular dynamics, the simplified distinct-conformer model, and the reduction of the solvent−solute interactions to the electrostatic potential. For example, our previous studies suggest that ab initio MD, impossible in this case, provides an unprecedented improvement of NMR parameters over classical MD.[34−36]

Finally, we should touch on the choice of model systems. We performed chiral-recognition NMR experiments on larger molecules not reported in the present study as well; the chiral NMR effect in these cases (e.g., α-pinene enantiomers, combination of α-pinene and 1-phenylethanamine) was immeasurably weak. On the other hand, chiral solvating agents (CSAs) providing larger shifts require specific substrate molecules[13] and are not suitable for a more universal chirality recognition. Thus, the small polar chiral molecules (Figure 1) appear as the best system for chirality monitoring so far. They mix and interact reasonably strongly with a variety of organic compounds. They also make the modeling easier, although fully satisfactory agreement with experimental data (Table 4) was not achieved. However, this can change quickly in the future as more accurate computational tools are available. We thus believe that the results convincingly demonstrate that developing a universal NMR methodology for chirality recognition, as based on combining an experiment with computations, is not an impossible task.

CONCLUSIONS

Chemical shifts sensitive to solvent chirality were detected experimentally for two chiral alcohols and one amine. Complex molecular dynamics and density functional computations revealed that the shift differences were to a large extent caused by the perturbation of conformer equilibria by the chirality, and a more direct solvent−solute interactions modeled via the average electrostatic potential. The analysis of MD trajectories allowed us to quantitatively estimate the implications for the chiral solvent−solute interactions for the structure of the first solvation sphere, i.e., in terms of the local solvent density and the radial distribution function. The magnitudes of the simulated differences in chemical shift corresponded well to the experiment, although detailed experimental trends could not be reproduced. Thus, although improvement of the computational methodology is desirable in the future, the simulations provided a useful insight into the mechanism of the chiral NMR splitting and chirality recognition in the solvent−solute interactions. The combination of the simulations with the experiment broadens future applications of NMR spectroscopy, including the absolute configuration determination of numerous compounds unable to form specific complexes with chiral NMR shift agents.

ASSOCIATED CONTENT

Supporting Information

Computational details from molecular dynamics are available free of charge via the Internet at http://pubs.acs.org.

AUTHOR INFORMATION

Corresponding Author

* E-mail: bour@uochb.cas.cz.

Notes

The authors declare no competing financial interest.

ACKNOWLEDGMENTS

The study was supported by the Academy of Sciences (M200551205), Grant Agency (P208/11/0105, 13-03978S) and Ministry of Education (LH11033, LM2010005, CZ.1.05/3.2.00/08.0144) of the Czech Republic.

REFERENCES

(1) Flack, H. D.; Bernardinelli, H. The Use of X-ray Crystallography to Determine Absolute Configuration. *Chirality* **2008**, *20*, 681−690.
(2) Barron, L. D. *Molecular Light Scattering and Optical Activity*; Cambridge University Press: Cambridge, 2004.
(3) Nafie, L. *Vibrational Optical Activity: Principles and Applications*; Wiley: Chichester, 2011.
(4) Wesolowski, S. S.; Pivonka, D. E. A Rapid Alternative to X-Ray Crystallography for Chiral Determination: Case Studies of Vibrational Circular Dichroism (VCD) to Advance Drug Discovery Projects. *Bioorg. Med. Chem. Lett.* **2013**, *23*, 4019−4025.
(5) Rogers, D. M.; Hirst, J. D. Calculations of Protein Circular Dichroism from First Principles. *Chirality* **2004**, *16*, 234−243.
(6) Harris, R. A.; Jameson, C. J. A Note on Chirality in NMR Spectroscopy. *J. Chem. Phys.* **2006**, *124*, 096101.
(7) Zanasi, R.; Pelloni, S.; Lazzeretti, P. Chiral Discrimination via Nuclear Magnetic Shielding Polarisabilities from NMR Spectroscopy: Theoretical Study of (R_a)-1,3-Dimethylallene, (2*R*)-2-Methyloxirane, and (2*R*)-*N*-Methyloxaziridine. *J. Comput. Chem.* **2007**, *28*, 2159−2163.
(8) Buckingham, A. D.; Fischer, P. Direct Chiral Discrimination in NMR Spectroscopy. *Chem. Phys.* **2006**, *324*, 111−116.
(9) Seco, J. M.; Quiñoá, E.; Riguera, R. The Assignment of Absolute Configuration by NMR. *Chem. Rev.* **2004**, *104*, 17−118.
(10) Parker, D. NMR Determination of Enantiomeric Purity. *Chem. Rev.* **1991**, *91*, 1441−1457.
(11) Wenzel, T. J. *Discrimination of Chiral Compounds Using NMR Spectroscopy*; John Wiley & Sons, Inc.: Hoboken, NJ, 2007.
(12) Wenzel, T. J.; Chisholm, C. D. Assignment of Absolute Configuration Using Chiral Reagents and NMR Spectroscopy. *Chirality* **2011**, *23*, 190−214.
(13) Pirkle, W. H.; Sikkenga, D. L. The Use of Chiral Solvating Agent for Nuclear Magnetic Resonance Determination of Enantiomeric Purity and Absolute Configuration of Lactones. Consequences of Three-Point Interactions. *J. Org. Chem.* **1977**, *42*, 1370−1374.
(14) Friebolin, H. *Basic One- and Two-Dimensional NMR Spectroscopy*; Wiley-VCH: Weinheim, 1998.
(15) Rinaldi, P. L. The Determination of Absolute Configuration Using Nuclear Magnetic-Resonance Techniques. *Prog. Nucl. Magn. Spectrosc.* **1982**, *15*, 291−352.
(16) Seco, J. M.; Quiñoá, E.; Riguera, R. Assignment of the Absolute Configuration of Polyfunctional Compounds by NMR Using Chiral Derivatizing Agents. *Chem. Rev.* **2012**, *112*, 4603−4641.
(17) Sullivan, G. R.; Dale, J. A.; Mosher, H. S. Correlation of Configuration and ^{19}F Chemical Shifts of α-Methoxy-α-Trifluoromethylphenylacetate Derivatives. *J. Org. Chem.* **1972**, *38*, 2143−2147.
(18) Wang, J.; Wolf, R. M.; Caldwell, J. W.; Kollman, P. A.; Case, D. A. Development and Testing of a General Amber Force Field. *J. Comput. Chem.* **2004**, *25*, 1157−1174.

(19) Case, D. A.; Cheatham, I. T. E.; Darden, T.; Gohlke, H.; Luo, R.; Merz, J. K. M.; Onufriev, A.; Simmerling, C.; Wang, B.; Woods, R. The Amber Biomolecular Simulation Programs. *J. Comput. Chem.* **2005**, *26*, 1668−1688.
(20) Pronk, S.; Páll, S.; Schulz, R.; Larsson, P.; Bjelkmar, P.; Apostolov, R.; Shirts, M. R.; Smith, J. C.; Kasson, P. M.; vanderSpoel, D.; et al. Gromacs 4.5: A High-Throughput and Highly Parallel Open Source Molecular Simulation Toolkit. *Bioinformatics* **2013**, *27*, 845−854.
(21) Kumar, S.; Bouzida, D.; Swendsen, R. H.; Kollman, P. A.; Rosenberg, J. M. The Weighted Histogram Analysis Method for Free-Energy Calculations on Biomolecules. I. The Method. *J. Comput. Chem.* **1992**, *13*, 1011−1021.
(22) Ham, S.; Kim, J. H.; Kochan, L.; Cho, M. Correlation between Electronic and Molecular Structure Distortions and Vibrational Properties. II. Amide I Modes of NMA−$n$$D_2O$ Complexes. *J. Chem. Phys.* **2003**, *118*, 3491−3498.
(23) Bouř, P.; Michalík, D.; Kapitán, J. Empirical Solvent Correction for Multiple Amide Group Vibrational Modes. *J. Chem. Phys.* **2005**, *122*, 144501.
(24) Frisch, M. J.; Trucks, G. W.; Schlegel, H. B.; Scuseria, G. E.; Robb, M. A.; Cheeseman, J. R.; Scalmani, G.; Barone, V.; Mennucci, B.; Petersson, G. A.; et al. *Gaussian 09*, revision D01; Gaussian, Inc.: Wallingford, CT, 2009.
(25) Tomasi, J.; Mennucci, B.; Cammi, R. Quantum Mechanical Continuum Solvation Models. *Chem. Rev.* **2005**, *105*, 2999−3093.
(26) Rappe, A. K.; Casewit, C. J.; Colwell, K. S.; Goddard, W. A., III; Skiff, W. M. UFF, a Full Periodic Table Force Field for Molecular Mechanics and Molecular Dynamics Simulations. *J. Am. Chem. Soc.* **1992**, *114*, 10024−10035.
(27) Grimme, S. Semiempirical GGA-Type Density Functional Constructed with a Long-Range Dispersion Correction. *J. Comput. Chem.* **2006**, *27*, 1787−1799.
(28) Becke, A. D. Density-Functional Thermochemistry. III. The Role of Exact Exchange. *J. Chem. Phys.* **1993**, *98*, 5648−5652.
(29) Ditchfield, R. Self-Consistent Perturbation Theory of Diamagnetism I. A Gauge-Invariant LCAO Method for N.M.R. Chemical Shifts. *Mol. Phys.* **1974**, *27*, 789−807.
(30) Klamt, A. COSMO and COSMO-Rs. In *The Encyclopedia of Computational Chemistry*; Schleyer, P. R., Allinger, N. L., Clark, T., Gasteiger, J., Kollman, P. A., Schaefer III, H. F., Schreiner, P. R., Eds.; John Wiley & Sons: Chichester, U.K., 1998; Vol. *1*; pp 604−615.
(31) Kutzelnigg, W.; Fleischer, U.; Schindler, M. *The IGLO-Method: Ab Initio Calculation and Interpretation of NMR Chemical Shifts and Magnetic Susceptibilities*; Springer: Heidelberg, 1990.
(32) DeCamp, M. F.; DeFlores, L.; McCracken, J. M.; Tokmakoff, A.; Kwac, K.; Cho, M.; Amide, I. Vibrational Dynamics of *N*-Methylacetamide in Polar Solvents: The Role of Electrostatic Interactions. *J. Phys. Chem. B* **2005**, *2005*, 11016−11026.
(33) Duan, Y.; Wu, C.; Chowdhury, S.; Lee, M. C.; Xiong, G. M.; Zhang, W.; Yang, R.; Cieplak, P.; Luo, R.; Lee, T.; et al. A Point-Charge Force Field for Molecular Mechanics Simulations of Proteins Based on Condensed-Phase Quantum Mechanical Calculations. *J. Comput. Chem.* **2003**, *24*, 1999−2012.
(34) Dračínský, M.; Möller, H. M.; Exner, T. E. Conformational Sampling by Ab Initio Molecular Dynamics Simulations Improves NMR Chemical Shift Predictions. *J. Chem. Theory Comput.* **2013**, *9*, 3806−3817.
(35) Dračínský, M.; Bouř, P. Computational Analysis of Solvent Effects in NMR Spectroscopy. *J. Chem. Theory Comput.* **2010**, *6*, 288−299.
(36) Dračínský, M.; Kaminský, J.; Bouř, P. Structure of Alanine Hydration Shell as Probed by NMR Chemical Shifts and Indirect Spin-Spin Coupling. *J. Phys. Chem. B* **2009**, *113*, 14698−14707.